

Study of nanocrystallization process in FeCrCuNbSiB amorphous alloys by Young's modulus measurements

N. BAYRI^{a*}, S. ATALAY^a, V. S. KOLAT^a, T. IZGI^a, P. SOVAK^b

^a*Inonu University, Science and Arts Faculty, Physics Department Malatya, Turkey*

^b*P.J. Safarik University, Department of Physics, Kosice, Slovakia*

This paper presents the influence of nanocrystallization process on magnetic field dependence of Young's Modulus of Fe_{74-x}Cr_xCu₁Nb₃Si₁₃B₉ (x=0, 2, 4, 8, 11) alloys. The samples were annealed between 450 °C and 600 °C for 1 hour under argon atmosphere to induce various nanocrystalline fractions. The variation in the microstructure upon annealing was examined by the X-ray spectrum data. Samples annealed at 500 °C or at higher temperature showed nanocrystalline α-Fe (Si) phase embedded in amorphous matrix. It was observed that the magnitude of field dependence of Young's modulus varies from 40% to a nearly zero as the saturation magnetostriction is reduced by nano size α-Fe(Si) grains. The results are interpreted partly in terms of internal stress relief and reduced magnetostriction in nanocrystalline samples.

(Received November 6, 2014; accepted September 9, 2015)

Keywords: Nanocrystalline materials, Young's modulus, magnetoelastic properties

1. Introduction

Nanostructure science and technology is a broad and interdisciplinary area of research and development activity that has been growing explosively worldwide in the past few years. It has the potential for revolutionizing the ways in which materials and products are created and the range and nature of functionalities that can be accessed. It is already having a significant commercial impact, which will assuredly increase in the future. One of the promising materials in this area is the soft ferromagnetic nanostructure materials.

The discovery of nanocrystalline Fe-based soft magnetic materials is less than twenty years old [1-2]. The first class of such materials was the melt-spun Fe-Si-B alloys containing small amounts of Nb and Cu [1, 2, 3]. The Fe-Si-B-Nb-Cu (Finemet) amorphous phase transforms to a body-centered cubic (bcc) Fe-Si solid solution with grain sizes of about 10 nm during annealing at temperatures above the crystallization temperature. The presence of small amounts of Cu helps increase the nucleation rate of the bcc phase while Nb retards the grain growth [2, 4, 5]. These "Finemet" alloys provide low core losses (even lower than amorphous soft magnetic alloys such as Co-Fe-Si-B), exhibit saturation induction of about 1.2 T, and exhibit very good properties at high frequencies, comparable to the best Co-based amorphous alloys. Another class of Fe-based nanocrystalline alloys was developed by Inoue and co-workers at Tohoku University [6]. These "Nanoperm" alloys are based on the Fe-Zr-B system; they contain larger concentrations of Fe (83-89 at.%) compared to the Finemet alloys (~ 74 at.% Fe) and have higher values of saturation induction (~ 1.6-1.7 T).

Magnetic field dependence of amorphous ferromagnetic materials [7-10] and the influence of substitution various alloying elements for Fe in FeCuNbSiB composition have been investigated [11-13]. It is known that additions of different elements to these systems can produce significant changes in their structural, magnetic and mechanical properties [12, 13]. It has been also reported that the partial substitution of Fe by Cr enhances the thermal stability of the amorphous alloy against nanocrystallization and lowers the Curie temperature of both, as-received glassy alloy and residual amorphous phase in nanocrystalline alloys [13-15]. We have previously reported effect of Cr content on the magnetic properties FeCrCuNbSiB alloys [13]. In this study, we have investigated the effect of the partial substitution of Cr for Fe in Fe_{74-x}Cr_xCu₁Nb₃Si₁₃B₉ (x=0, 2, 4, 8, 11) alloys on nanocrystallization process using ΔE effect, magnetostriction and M-H loops measurements. Magnetic field dependence of the Young's modulus measurements (ΔE effect) are interpreted on the basis of a phenomenological model [16] and discussed in the light of existing ideas about the nanocrystallization process.

2. Theoretical Model

In field-annealed amorphous ribbons the domain structure is simple, and the modeling of the ΔE effect for various easy axis orientations is straightforward [16]. The Young's modulus can be expressed in the form [16];

$$E/E_s = 1 / (1 + \lambda_s^2 E_s F(\theta, H, \sigma) / K) \quad (1)$$

where E_s is the saturation modulus, λ_s is the saturation magnetostriction, and K is the anisotropy constant. F is a

numerical factor whose maximum value is of order unity, and is a function of the easy-axis orientation (θ), applied "field H , and stress, σ ". The magnitude of the ΔE effect is thus seen to be determined mainly by the dimensionless ratio, $\beta = \lambda_s^2 E_s / K$. The variation of normalized Young's modulus obtained from Eq. 1 is given in Fig.1. The particular features of these curves that are important for interpreting the results reported in this article are the following: (a) the value of the modulus ratio at $H=0$, denoted by E_0/E_s , equals 1 only in the special case where all moments are initially at right angles to the field axis; this state can be closely achieved in ribbons by transverse field annealing. (b) For easy axis angles between 90° and 45° , E_0/E_s , decreases monotonically. (c) For angles greater than 45° the modulus at first decreases with increasing H , reaching a minimum value denoted by E_{\min}/E_s . For angles between 0° and 45° there is no decrease in modulus, so $E_{\min}/E_s = E_0/E_s$, (d) the value of E_{\min}/E_s is determined predominantly by the ratio β defined above. Since λ_s and E_s may be assumed to be approximately constant during annealing, the changes in E_{\min}/E_s are primarily related to changes in the anisotropy constant K : the lower the value of K , the lower the value of E_{\min}/E_s (e) For easy axis directions that vary throughout the sample the modulus changes can be calculated as the weighted average of the modulus over the range of angles. In particular, any easy axes at angles intermediate between 0° and 90° to the axis will result in a value of E_0/E_s , less than 1, and any easy axes at angles greater than 45° to the axis will cause an initial drop in modulus with applied field, so that $E_{\min}/E_s < E_0/E_s$.

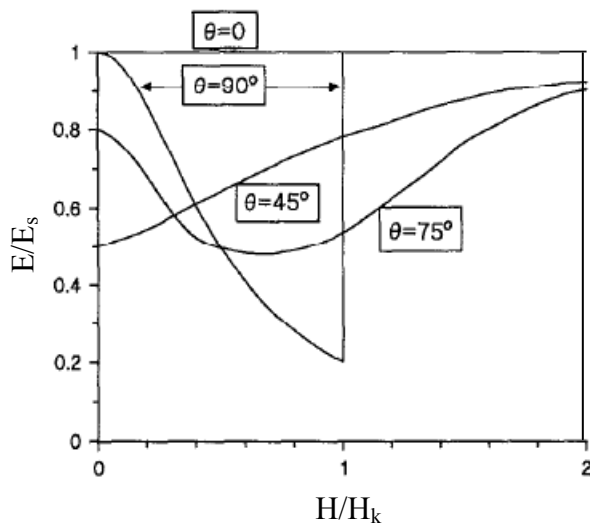


Fig.1. The field dependence of Young's modulus calculated from Squire [16]. The field is normalized to the anisotropy field $H_k = 2K/\mu_0 M_s$ and the Young's modulus to its saturation value, E_s .

3. Experimental details

Amorphous $Fe_{74-x}Cr_xCu_1Nb_3Si_{13}B_9$ ($x = 0, 2, 4, 8, 11$) ribbons were prepared by the melt-spinning technique. The crystallization behaviours of the samples were investigated by DTA-50 Shimadzu differential thermal analyzer. Thermal data were measured at the heating rates of 5, 10, 15, 20 $^\circ C/min$. The thermal treatments were carried out at various temperatures for 1 h under argon atmosphere. The sample has a thickness of $\sim 23 \mu m$. The samples were cut into sizes 4 cm long and 0.5 cm wide. The glass structure of as-received samples was confirmed by X-ray powder diffraction (Rigaku-Radb) measurements using CuK_α radiation. In X-ray measurements, X-ray power and scanning rate were set at 30 kV, 15mA and " $1^\circ min^{-1}$ ", respectively. Also, the changes in the microstructure upon annealing were examined by XRD. The grain size was calculated using Scherrer formula, which given in Eq. 2. The grain size, D , of α -Fe(Si) was estimated from the full-width at half-maximum (FWHM) of the diffraction peak of α -Fe(Si) using Eq. 2 after correction of instrumental broadening [17]. In the calculation of grain size, a Gauss curve for amorphous peak and a Lorentz curve were fitted.

$$D = \lambda / (FWHM \cos \theta) \quad (2)$$

where λ is the wavelength of X-ray and θ the Bragg angle. The $M-H$ curves were measured at dc. The ΔE effect was measured by the vibrating reed method [18], with the third mode excited with a free length of 1.5 cm. The values of Young's modulus are normalised to the modulus value at maximum applied field, E_s . The field dependence of magnetostriction, λ , was measured using a fibre-optic dilatometer [19].

4. Results

Cr concentration dependence of the peak value of onset crystallization temperatures T_{x1} and T_{x2} of α -Fe(Si) phase formed in the first stage of crystallization and of the boride type phases formed in the second stage, respectively, were obtained using DTA with a heating rate of 5 $^\circ C/min$ (Fig.2). The first onset crystalline temperatures (T_{x1}) for $Fe_{74-x}Cr_xCu_1Nb_3Si_{13}B_9$ ($x = 0, 2, 8, 11$) samples were observed at 502.5 $^\circ C$, 518.7 $^\circ C$, 525.7 $^\circ C$ and 550.1 $^\circ C$, respectively. The second onset crystallization temperatures (T_{x2}) of %2 and %11 Cr doped samples were assured as 664.3 $^\circ C$ and 658.1 $^\circ C$, respectively.

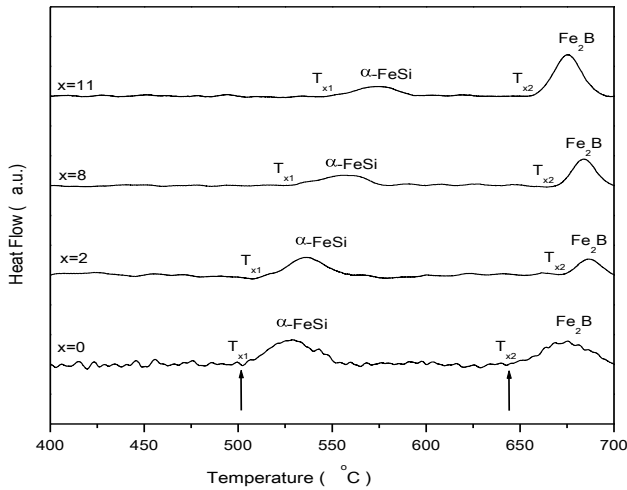


Fig.2. DTA curves of $Fe_{74-x}Cr_xCu_1Nb_3Si_{13}B_9$ samples.

An increase in T_{x1} and very small decrease in T_{x2} were observed with increasing Cr content. The activation energy of the crystallisation process gives important information about the thermal stability of the sample [20-22]. Therefore, it is important to know the activation energy of the crystallization process. The activation energies for crystallisation of the $Fe_{74-x}Cr_xCu_1Nb_3Si_{13}B_9$ ($x=0, 2, 4, 8, 11$) alloys were determined from the DTA curves through the well-known Kissinger [23] is,

$$\ln\left(\frac{\beta}{T_p^2}\right) = -\frac{E_a}{RT_p} + \text{const} \quad (3)$$

where β is the heating rate, T_p is the temperature at the exothermal peak, R is the gas constant, and E_a is the activation energy of crystallization.

The thermal data were also measured at heating rates of 5, 10, 15, 20 °C/min to obtain activation energy (Fig.3). The results showed that the addition of Cr for Fe first increases the activation energy up to 518 kJ/mol and then decreases when the Cr content is higher than 11%. Amorphous and nanocrystalline state of samples have been studied by X-ray diffraction. The average grain diameters of α -Fe(Si) crystallites calculated from Eq. 2 are about 17 nm for 2% Cr content, 12 nm for 8% Cr content,

9 nm for 11% Cr content and 2–3 nm for 14% Cr content in the alloys annealed at 550 °C for 1 h. The sample with 17% Cr shows fully amorphous structure. The X-ray data also confirms that the Cr produces a slowing down of nanocrystallization kinetics and smaller mean grain size of the α -Fe(Si) phase. Figure 4 shows X-ray diffraction patterns of $Fe_{72}Cr_2Cu_1Nb_3Si_{13}B_9$ alloys annealed at 450, 500, 550 and 600 °C for 1 h. As shown at Fig.4, sample annealed at 450 °C has mostly amorphous phase, the small peaks observed could be due to Cu phase. For the sample annealed at 500 °C, it was determined that Cu clusters have occurred at the interface of the remaining amorphous phase and the α -Fe(Si) phase. After annealing at 550 °C the structure is composed of amorphous matrix, α -Fe(Si) phase and Fe_3Si phase. On the other hand for the sample annealed at 600 °C, α -Fe(Si), Fe_3Si and Fe_2B phases were observed. The average grain size of α -Fe(Si) crystallites increase from 6 to 21 nm with increasing annealing temperature. X-ray results clearly indicated that as-prepared and samples annealed below 450 °C has amorphous structure, annealing of sample above 500 °C, first Cu clusters form in the sample and it has been reported that these clusters leads to growth of α -Fe(Si) phase in the amorphous matrix [1, 24-26].

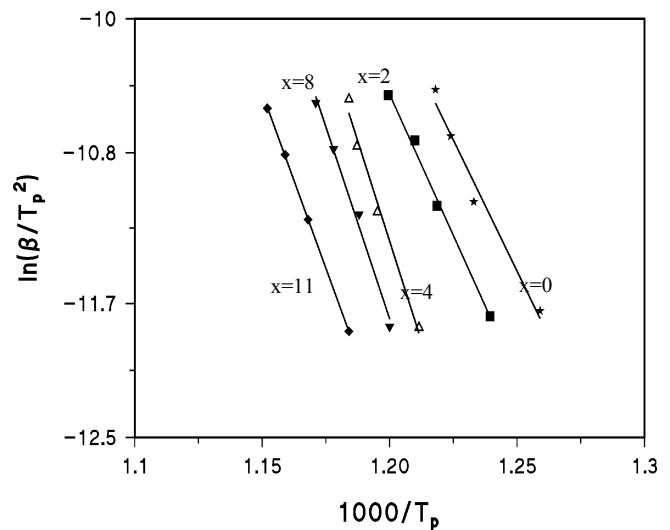


Fig.3 Kissinger plots of $Fe_{74-x}Cr_xCu_1Nb_3Si_{13}B_9$ samples.

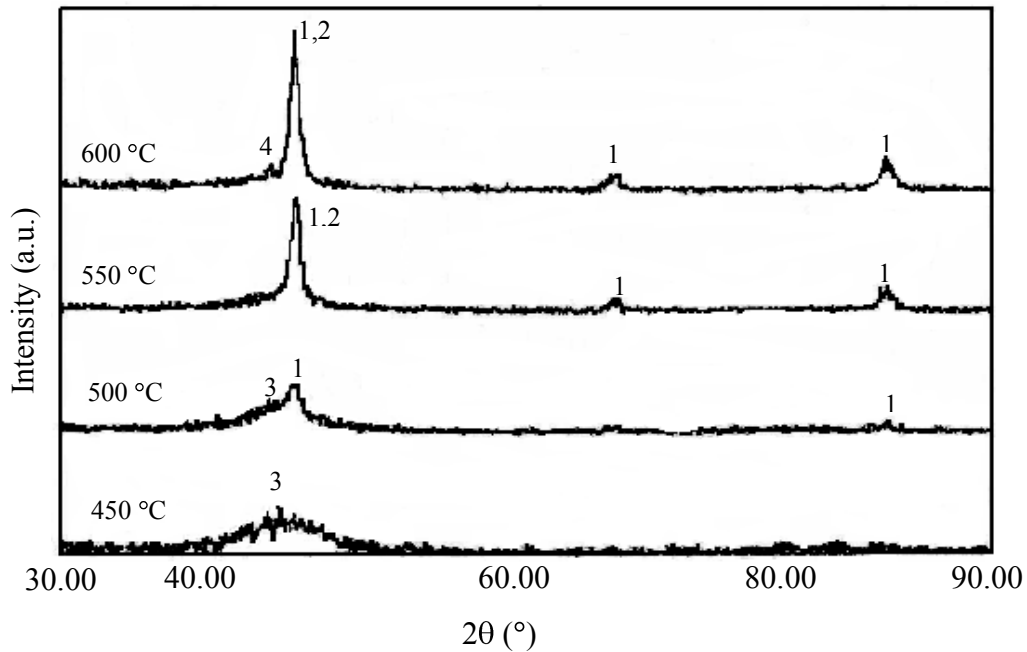


Fig.4. X-ray spectrum of $Fe_{72}Cr_2Cu_1Nb_3Si_{13}B_9$ sample annealed at various temperatures, 1: α -FeSi phase; 2: Fe_3Si phase; 3: Cu phase; 4: Fe_2B phase.

Fig. 5 shows magnetization loops for $Fe_{72}Cr_2Cu_1Nb_3Si_{13}B_9$ alloy as a function of annealing temperature. Fig. 6 shows field dependence of the magnetostrictive strain (λ_e) for $Fe_{72}Cr_2Cu_1Nb_3Si_{13}B_9$ samples annealed at temperatures 450, 500 and 550 °C. Fig. 7 shows maximum magnetostrictive strain (λ_{peak}) for $Fe_{74-x}Cr_xCu_1Nb_3Si_{13}B_9$ ($x = 0, 2, 8, 11$) samples as a function of annealing temperature. Maximum magnetostrictive strain first slowly then sharply decreases with increasing annealing temperature, as it is stated above the sharp decrease is due to the formation of α -Fe(Si) crystallites. At higher temperatures, an increase in the maximum magnetostrictive strain for $x=0$ sample was observed. This is due to formation of Fe_2B phase in the sample. DTA results clearly shows that Fe_2B phase for $x=0$ sample forms at lower temperature considering samples with higher Cr content. Therefore, maximum magnetostrictive strain of $x=0$ sample increases at 600°C relative to other composition. Figs. 8 and 9 show normalized $E(H)$ curves of $Fe_{74-x}Cr_xCu_1Nb_3Si_{13}B_9$ ($x = 2$ and 8) samples annealed at various temperatures.

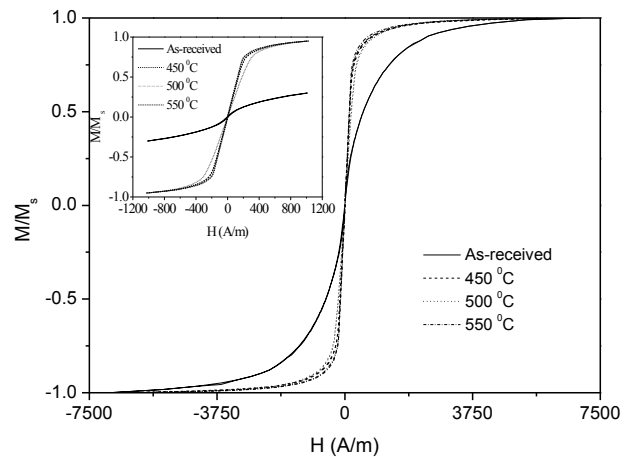


Fig.5. $M-H$ loops of $Fe_{72}Cr_2Cu_1Nb_3Si_{13}B_9$ sample annealed at various temperatures. Inset shows same curves at low magnetic field region.

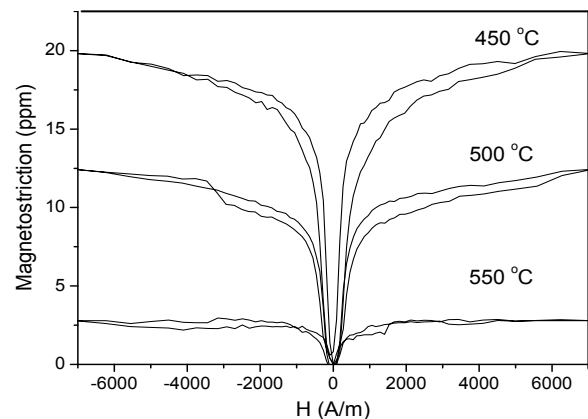


Fig.6. Variation of magnetostriction values of $Fe_{72}Cr_2Cu_1Nb_3Si_{13}B_9$ sample annealed at various temperatures.

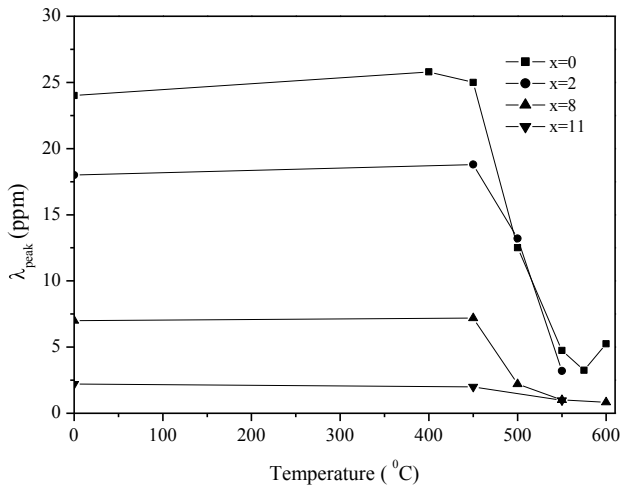


Fig. 7. Peak value of magnetostriction of $Fe_{74-x}Cr_xCu_1Nb_3Si_{13}B_9$ samples as a function of annealing temperature.

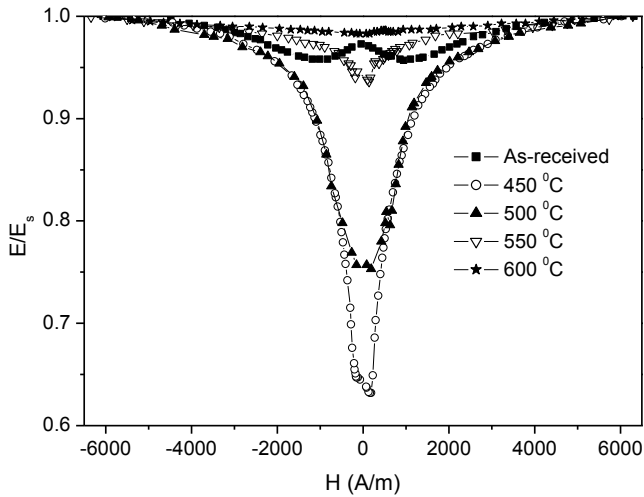


Fig. 8. Normalised Young's modulus of $Fe_{72}Cr_2Cu_1Nb_3Si_{13}B_9$ samples annealed at various temperatures.

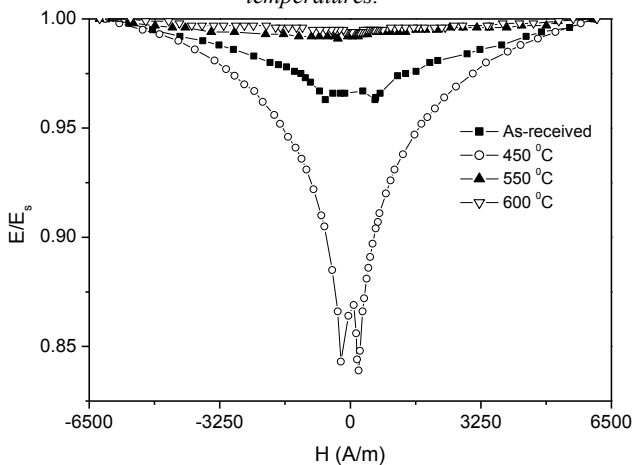


Fig. 9. Normalised Young's modulus of $Fe_{66}Cr_8Cu_1Nb_3Si_{13}B_9$ samples annealed at various temperatures.

5. Discussion

All samples behave similarly with respect to annealing temperature. Annealing temperature, T_a , can therefore be divided into three ranges; in the first range ($0 < T_a < 450^\circ C$) all samples show amorphous structure. At this range, coercivity decreases with T_a . λ_{peak} , which is given by $\lambda_{peak} = 3/2 \lambda_s \sin^2\theta$, where λ_s is the saturation magnetostriction constant and θ is the angle between the easy axis and applied magnetic field, does not appreciably change with respect to the as-received value. The λ_s of nanocrystalline alloy can be expressed as;

$$\lambda_s = v_{cry} \lambda_s^{cry} + (1 - v_{cry}) \lambda_s^{am} \quad (4)$$

where v_{cry} is the volume fraction of the crystalline phase and λ_s^{am} and λ_s^{cry} are the magnetostriction of the amorphous and crystalline phases respectively. For nanocrystalline alloy, the λ_s^{am} is positive and λ_s^{cry} is negative for Fe(Si) phases [27, 28]. Saturation magnetostriction values (λ_s) of α -Fe(Si), Fe_3Si and Fe_2B phases in nanocrystalline alloy was determined as -6×10^{-6} , -9.3×10^{-6} and 15.6×10^{-6} respectively [29]. The formation of the nanocrystalline Fe(Si) phases leads to the reduction of magnetostriction [27, 29]. At the second range of annealing temperature ($450^\circ C < T_a < 600^\circ C$), where the α -Fe(Si) and Fe_3Si phases are formed, coercivity and λ_{peak} go to minimum values as a function of annealing temperature, leading to optimum magnetic properties [27, 29]. It was also observed that the addition of Cr leads to a decrease in the minimum value of coercivity and λ_{peak} . Over the final range of annealing temperature range ($600^\circ C < T_a < 650^\circ C$), a large increase in H_c and a small increase in λ_{peak} were observed. This large increase of H_c and a small increase in λ_{peak} is due to the formation of the Fe_2B phase with large magnetocrystalline anisotropy.

The magnitude of the ΔE effect firstly increases and then decreases with increasing Cr content for as-received samples. This behaviour can be understood by considering the dimensionless quantity, $\beta = \lambda_s^2 E_s / K$ which is given in the theoretical model [16] section. It can be shown that $\beta = (E_s / E(H) - 1) / F$. For the data considered here, F can be taken as about 1. It is well known that in as-quenched state, the sample has a large residual stress, which combines with the magnetostriction to produce relatively high anisotropy. Therefore the magnitude of ΔE effect for the as-received samples is very small. The as-received sample with 2 % Cr content shows bigger change than sample with 8 % Cr content, because λ_s in the β parameter is much higher for the sample with 2 % Cr content. The X-ray and DTA results showed that the samples annealed below $450^\circ C$ do not have nanocrystalline phase (see Fig. 2 and 4). The increase in the magnitude of ΔE effect of the samples annealed at $450^\circ C$ can therefore be attributed entirely to stress relief, and consequently decrease in K.

In the samples with $x=0, 2, 4$ Cr content annealed at the second range of annealing temperature ($450\text{ }^{\circ}\text{C} < T_a < 600\text{ }^{\circ}\text{C}$), a large decrease in the magnitude of ΔE effect was observed. This is probably due to the large reduction in the magnetostriction (see Fig. 6 and 7) or large increase in K . M-H loops measurements show that sample annealed at the second range have very small K showing that the magnetocrystalline anisotropy rises from the α -Fe(Si) or Fe_3Si nanocrystalline phases aligns in a random direction in a way that the total average magnetocrystalline anisotropy becomes nearly zero. In conclusion, the large decrease in the magnitude of ΔE effect at the $450\text{ }^{\circ}\text{C} < T_a < 600\text{ }^{\circ}\text{C}$ ranges can be related to only the reduction of magnetostriction value. On the calculations of $\beta = \lambda_s^2 E_s / K$ indicated that for samples with 2% and 4% Cr content, the reduction in magnetostriction is the reason for the decrease in the magnitude of ΔE effect. But for the samples with 8% or higher Cr content, both reduction in magnetostriction and increase in K are responsible for the large decrease in the magnitude of ΔE effect. This large increase in K , which is due to the formation of boride phases (see Fig.2 and 4), for these samples was also observed in M-H data. No ΔE effect was observed in the samples annealed at $600\text{ }^{\circ}\text{C}$ due to large intergrain magnetocrystalline anisotropy.

One additional information which can be drawn from Figs. 8 and 9, is that the easy axis distribution appears to be little affected by annealing. This is shown by the nearly consistent shape of the $E(H)$ curves. A small minimum was observed in the E/E_s curves of samples annealed between $400\text{ }^{\circ}\text{C}$ and $550\text{ }^{\circ}\text{C}$. Therefore, the easy axis distribution appears to be little affected by annealing. The comparison of the shape of E/E_s curves of the theoretical model [16] with experimental data also show that the average easy axis angle of magnetization is around 45° with respect to the ribbon axis. The E/E_s curve of the sample annealed at $600\text{ }^{\circ}\text{C}$ does not show any minimum; E increases with increasing H . This suggest that easy average easy axis orientation of magnetic moments is smaller than 45° .

6. Conclusion

In FeCrCuNbSiB samples, substitution of Cr lowers the magnetization, magnetostriction and coercive field values, also suppresses nucleation of α -Fe(Si) phase. Samples annealed at $500\text{ }^{\circ}\text{C}$ or at higher temperature showed nanocrystalline α -Fe(Si) phase embedded in amorphous matrix. It was observed that the magnitude of field dependence of Young's modulus varies from 40% to a nearly zero as the saturation magnetostriction is reduced by nano size α -Fe(Si) grains.

The measurement of ΔE also allowed us to estimate the compositional dependence of effective anisotropy

energy, particularly in as-received FeCrCuNbSiB samples. From these results we can conclude that the partial substitution of Fe by Cr could lead to a magnetic softness for small Cr contents.

Acknowledgements

This work was supported by Inonu University with project number 2012/37.

References

- [1] Y. Yoshizawa, S. Oguma and K. Yamauchi, *J. Appl. Phys.* **64**, 6044 (1988).
- [2] G. Herzer, *IEEE Trans. Magn.* **25**, 3327 (1989).
- [3] G. Herzer, *IEEE Trans. Magn.* **26**, 1397 (1990).
- [4] V. Franco, C.F. Conde, A. Conde, B. Varga, A. Lovas, *J. Magn. Mater.* **215-216**, 404 (2000).
- [5] P. Marin, M. Lopez, A. Hernando, Y. Iqbal, H.A. Davies, M.R.J. Gibbs, *J. Appl. Phys.* **92**, 374 (2002).
- [6] A. Makino, A. Inoue and T. Masumoto, *Nanostructured Materials* **6**, 985 (1995).
- [7] S. Atalay, P.T. Squire, M.R.J. Gibbs, *IEEE Trans. Magn.* **29**, 3472 (1993).
- [8] D. Atkinson, P.T. Squire, M.R.J. Gibbs, S. Atalay, *J. Appl. Phys.* **73**, 3411 (1993).
- [9] S. Atalay, P.T. Squire, *J. Appl. Phys.* **73**, 871 (1993).
- [10] S. Atalay, P.T. Squire, *Measur. Sci. Tech.* **3**, 735 (1992).
- [11] M. Ohnuma, D.H. Ping, T. Abe, H. Onodera, K. Hono, Y. Yoshizawa, *J. Appl. Phys.* **93**, 9186 (2003).
- [12] P. Minguez, H.A. Davies, I. Todd, M.R.J. Gibbs, A. Garcia-Arribas, J. Gutierrez, *J. Non-Cryst. Solids* **287**, 428 (2001).
- [13] N. Bayri, H.I. Adiguzel, S. Atalay, P. Sovak, *Phys. Stat. Sol. (a)* **189**, 805 (2002).
- [14] N. Murillo, J. Rodriguez, I. Etxebarria, J. Gonzalez, *J. Magn. Mater.* **272-276**, 1471 (2004).
- [15] A.K. Panda, I. Chatteraj, A. Mitra, *J. Magn. Mater.* **222**, 263 (2000).
- [16] P. T. Squire, *J. Magn. Mater.* **87**, 299 (1990).
- [17] E.F. Kaelble, *Handbook of X-rays*, McGraw-Hill, New York, 1967.
- [18] S. Atalay, PhD Thesis, University of Bath, U.K. (1991).
- [19] P.T. Squire, M.R.J. Gibbs, *J. Phys. E* **20**, 499 (1987).
- [20] C. Yang, Q.R. Cheng, L.H. Liu, Y.H. Li, Y.Y. Li, *Intermetallics*, **56**, 37 (2015).
- [21] L.M. Zou, Y.H. Li, C. Yang, S.G. Qu, Y.Y. Li, *J. Alloys and Compd.* **553**, 40 (2013).
- [22] C. Yang, L.H. Liu, Y.G. Yao, Y.H. Li, Y.Y. Li, *J. Alloys and Compd.* **586**, 542 (2014).

- [23] H.E. Kissinger, J. Res. NBS **57**, 217 (1956).
- [24] K. Hono, D.H. Ping, M. Ohnuma, H. Onodera, Acta Mater. **47**, 997 (1999).
- [25] J.S. Blazquez, V. Franco, A. Conde, J. Phys.: Condens. Matter **14**, 11717 (2002).
- [26] J.S. Blazquez, J.M. Borrego, C.F. Conde, A. Conde J.M. Greneche, J. Phys.: Condens. Matter **15**, 3957 (2003).
- [27] G. Herzer, Mater. Sci.Eng. A **133**, 1 (1991).
- [28] H.R. Lasgari, D. Chu, S. Xie, H. Sun, M. Ferry, S. Li, J. Non-Crys. Solids **391**, 61 (2014).
- [29] G. Vlasak, P. Svec, D. Janickovic, Mater. Sci.Eng. A **375-377**, 1149 (2004).

*Corresponding author: nevzat.bayri@inonu.edu.tr